

Absolute negative mobility in a vibrational motor

Luchun Du* and Dongcheng Mei

Department of Physics, Yunnan University, Kunming 650091, China

(Received 28 June 2011; revised manuscript received 1 December 2011; published 30 January 2012)

An anomalous transport phenomenon termed absolute negative mobility (ANM) was observed in a vibrational motor, where an additional time-periodic signal filled the role usually played by noise in a Brownian motor. Within a tailored parameter regime, the ANM behavior is maximized at two regimes upon variation of the bias. The observed ANM still survives at a wide range of the driving strength and angular frequency of the additional signal.

DOI: [10.1103/PhysRevE.85.011148](https://doi.org/10.1103/PhysRevE.85.011148)

PACS number(s): 05.60.Cd, 05.45.-a

I. INTRODUCTION

Directed transport in a periodic structure was investigated extensively due to its potential applications in many processes of physics, chemistry, and biology [1–7]. A Brownian motor provides a prominent example for the constructive role of nonequilibrium fluctuations. One can extract usable work from noise based on the mechanism of a Brownian motor. Recently, an alternative and surprising phenomenon termed absolute negative mobility (ANM) stimulated extensive research [8–17]. The ANM phenomenon involves a paradoxical migration mechanism in which particles always move in a direction opposite to the net acting force [10–13]. At first sight it may conflict with the second law of thermodynamics and the principle of Le Chatelier. However, for a system driven far away from equilibrium by a time-periodic force, the onset of ANM is possible. Initially, ANM is based on genuine quantum-mechanical effects [8]. Subsequent research revealed the performance of ANM under the realm of classical physics [9–17]. The classical ANM was observed first in a spatially periodic and symmetric model of interacting Brownian particles [9], then it was further detected where a single Brownian particle was forced along meandering paths in a suitably tailored channel with inner walls [10–13].

Recently, ANM has been theoretically and experimentally studied in the simplest case of a single Brownian particle dynamics in one dimension [14–19]. The ANM phenomenon of a purely noise-induced type will be maximized for an appropriate amount of noise [14], while the deterministic ANM induced by transient chaos will be weakened and diminished by increasing temperature [15,16]. Inertial effects and high frequency driving are vital for the occurrence of ANM [14–17]. The absolute negative conductance (ANC) phenomenon in a Josephson junction device constitutes a realistic example of the ANM in the general systems [18,19]. Furthermore, ANM may arise as a special case when an overdamped Brownian particle is exposed to a two-dimensional square lattice potential [20]. The spatial asymmetry in the geometry of the transported particle is able to cause ANM in a periodically segmented two-dimensional channel [21]. In the presence of time-delayed feedback, a spatially symmetric and periodic system may show some character of the negative mobility in an overdamped regime [22]. The interaction of two coupled

particles can stimulate negative mobility in an overdamped periodic system [23]. A new sorting and fractionation method for colloidal particles in a periodically structured microfluidic device has been successfully utilized based on the mechanism of ANM [24].

Existing works about the classical ANM phenomenon are always related to noise effects [9–23]. Motivated by research on vibrational resonance where the role of noise in stochastic resonance is replaced by a time-periodic signal [25,26], here an alternative scenario is proposed to produce ANM. It is interesting to investigate whether the ANM phenomenon can exist when a time-periodic driving replaces the noise in the Brownian motor exhibiting ANM [14–17]. This strategy is technically feasible and may have promising applications [26,27]. According to the terminology about vibrational resonance, the periodic system is referred to as a “vibrational motor” where a time-dependent signal plays a similar role as the noise in the nonequilibrium transport process.

This paper is arranged as follows. In Sec. II, the dynamical equation for a vibrational motor is introduced and the average velocity is simulated and discussed. In Sec. III, a conclusion of the results ends the paper.

II. ABSOLUTE NEGATIVE MOBILITY IN A VIBRATIONAL MOTOR

An inertial particle in a spatially symmetric periodic potential under the influence of two time-periodic signals and a constant bias is governed by the dynamical equation expressed in dimensionless form

$$\ddot{x} + \gamma \dot{x} = -V'(x) + a \cos(\omega t) + A \cos(\Omega t + \phi) + f, \quad (1)$$

where $x = x(t)$ is a position of the particle at time t , a dot and prime denote differentiation with respect to t and x , respectively. The parameter γ denotes the friction coefficient. The external spatially symmetric periodic potential reads $V(x) = \sin(2\pi x)$ with unit period and barrier height $\Delta V = 2$. $a \cos(\omega t)$ denotes the first time-periodic signal with frequency ω and of amplitude a . $A \cos(\Omega t + \phi)$ is the second time-periodic signal with frequency Ω and amplitude A . ϕ controls the relative phase shift between the two time-periodic forces. f is the constant bias force which can be negative, zero, or positive.

Equation (1) represents the archetypal model of a vibrational motor. The first time-periodic force is strong and can bring the system out of equilibrium. The second time-periodic

*dulch@126.com

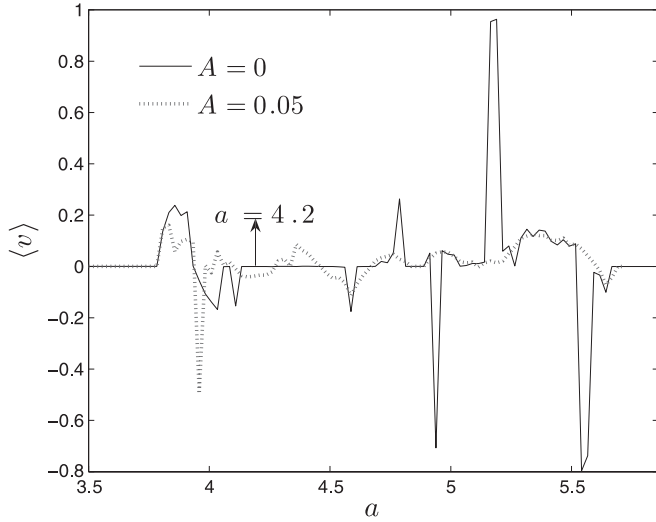


FIG. 1. The average velocity $\langle v \rangle$ of an inertial particle described by Eq. (1) is depicted as a function of the forcing amplitude a for the monochromatic (solid line) and biharmonic (dotted line) dynamics. The remaining parameters are $f = 0.12$, $\omega = 4.9$, $\gamma = 0.9$, $\Omega = 1.6$, and $\phi = 0$.

signal is weak and creates analogous effects as noise. For the absence of the second signal, the corresponding system exhibits very rich dynamical behaviors, such as periodic, quasiperiodic, and chaotic motion in the asymptotic long time limit [28–30]. Within the proper parameter regime different attractors may coexist. In the presence of the second signal, by manipulating its driving amplitude and frequency, some anomalous transport phenomena can be observed.

The inertia term \ddot{x} in Eq. (1) is an indispensable ingredient for the ANM phenomenon. Inertial effects play a crucial role for this anomalous transport feature [14]. The ANM is strictly ruled out in the absence of the inertia term [16]. The first time-periodic driving is also indispensable since the ANM only survives in the nonequilibrium environment. Our study focuses on the parameter regime that will never be reached by the basins of transporting attractors with opposite velocities. Without the second time-periodic driving, the system dynamics is only governed by the nontransporting attractors and the average velocity is always zero. Therefore the second signal is vital for the emergence of ANM. A modification on the second signal is allowable, for example, one can change it into a square-wave signal. Lastly, omitting the dissipative term $\gamma\dot{x}$ will not exclude the ANM phenomenon in principle. But the ANM phenomenon in the Hamiltonian limit is beyond the scope of this paper.

If the last term of Eq. (1) is a noise [14–17], the transitions between any deterministic attractor are always ergodic due to noise-induced metastability. Hence the velocity is independent of the initial condition. However, when the last term is a time-periodic signal, Eq. (1) is purely deterministic so that the resulting asymptotic long time dynamics is not necessarily ergodic [17]. Particularly, solutions of different types and with different transport directions (in the direction of f or opposite to f) may coexist within a tailored parameter region. Different initial conditions may result in different types of solutions.

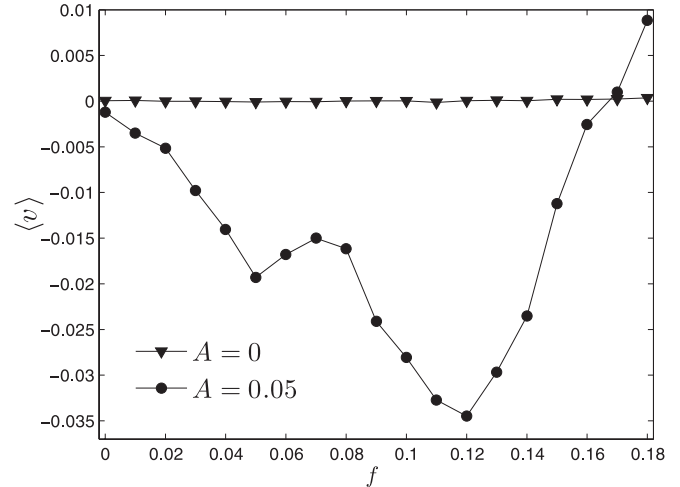


FIG. 2. The average velocity $\langle v \rangle$ of an inertial particle described by Eq. (1) depicted versus the external bias f for the monochromatic (triangles) and biharmonic (circles) dynamics. The remaining parameters are $a = 4.2$, $\omega = 4.9$, $\gamma = 0.9$, $\Omega = 1.6$, and $\phi = 0$.

Under such a condition, an additional average over the initial conditions must be performed.

The velocity $\langle v \rangle$ averaged over the time and ensemble is used to characterize the directed transport in the vibrational motor. It is defined as [16]

$$\langle v \rangle \equiv \frac{\tau}{L} \left\langle \lim_{t \rightarrow \infty} \frac{1}{t} \int_0^t dt' \dot{x}(t') \right\rangle, \quad (2)$$

where the ensemble average is indicated by $\langle \cdot \rangle$ and the time average ensures the independence of the initial transients. $\tau = \frac{2\pi}{\omega}$ denotes the temporal periodic of the first driving force while $L = 1$ is the spatial periodic of the potential structure. We carried out comprehensive numerical simulations of Eq. (1) by the Runge-Kutta method of the second order with time step $\Delta t = 0.001$. The ensemble average is taken over an ensemble of $N = 1000$ trajectories with uniformly distributed initial conditions of position. For each trajectory the simulation time interval is taken as $T_s = 3 \times 10^5$. The driving frequency $\omega = 4.9$ of the first signal and friction coefficient $\gamma = 0.9$ are fixed throughout the paper. Specifically, $a = 4.2$, $\omega = 4.9$, $\gamma = 0.9$ are restricted in Figs. 2 through 5. This is a set of optimal parameter values for the emergence of noise-induced ANM [14]. The ANM induced by the additional signal is expected to appear in this regime. Parts of our results are presented as follows.

Figure 1 depicts the dependence of the average velocity $\langle v \rangle$ versus the driving amplitude a of the first signal for a positive bias set at $f = 0.12$. One can see that the particle exhibits the behaviors of normal positive transport ($\langle v \rangle > 0$), zero transport ($\langle v \rangle = 0$), and anomalous negative transport ($\langle v \rangle < 0$) for different values of a . We are interested in the regime where $\langle v \rangle = 0$ for the monochromatic signal driving ($A = 0$) and $\langle v \rangle < 0$ for an additional signal driving ($A = 0.05$). The corresponding ANM phenomenon occurs taking $a = 4.2$ as an example. This ANM behavior is solely induced by the additional signal where it was identified by noise in a Brownian motor in the same parameter regime [14,16,18].

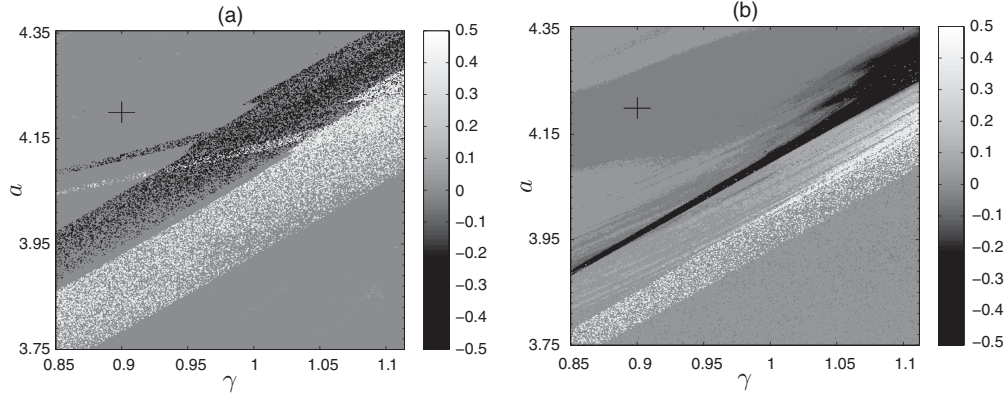


FIG. 3. The (γ, a) plane for the case of the coexisting $v = 0$ and $v = \pm \frac{1}{2}$ attractors. Different gray tones denote different velocities. The white regime corresponds to the attractor $v = \frac{1}{2}$ while the black region denotes the attractor $v = -\frac{1}{2}$. The parameters are chosen as $\omega = 4.9$, $f = 0.12$, $\Omega = 1.6$, $\phi = 0$ and (a) $A = 0$, (b) $A = 0.05$. The particular choice of the parameter values ($a = 4.2$ and $\gamma = 0.9$) in Figs. 1, 2, and 4 is indicated by a black cross.

A typical example for the ANM phenomenon is displayed in Fig. 2. The average velocity $\langle v \rangle$ against the external bias f is plotted within particular parameter regimes ($a = 4.2$, $\omega = 4.9$, $\gamma = 0.9$) where ANM can be solely induced by noise [14,16,18]. The average velocity is zero for small f without the second signal ($A = 0.00$) (i.e., the system is at a locked state that does not contribute to the directed transport). However, the presence of the second periodic driving changes this picture. A very weak driving strength yields a negative velocity for $f \leq 0.17$. The particle displays normal transport by further increasing f . It should be pointed out that the average velocity $\langle v \rangle$ posses two negative-valued minima at $f = 0.05$ and $f = 0.12$, respectively. From the physical viewpoint, the ANM effect is enhanced by f in two different regimes. To our best knowledge it has not been observed in the previous works concerning the ANM phenomenon in the one-dimensional periodic potential. This behavior has been observed before for a single particle moving in a zigzag-shaped two-dimensional potential pipeline [11].

To provide in more detail the nature of the ANM in the vibrational motor, let us look at orbits just for the absence and presence of the second signal. For the absence of the second driving force (i.e., $A = 0$) the orbit is at a locked state that does not contribute to the directed transport. Consequently, the average velocity $\langle v \rangle$ at $A = 0$ for varying f in a small range is zero. There exist a large number of unstable periodic orbits, transporting the particle in both positive and negative directions [14]. In the presence of the second signal the orbit is divided into two parts. The first part displays an almost regular oscillated motion and the second parts exhibits intermittent bursts into the negative direction. As a consequence, the average velocity $\langle v \rangle$ is negative at $A = 0.05$ for $f > 0$.

The role of the coexisting attractors is essential for the ANM phenomenon [15,16,18,19]. In Fig. 3, the coexisting attractors are demonstrated for bias force $f = 0.12$. Equation (1) is integrated numerically for different values of γ and a by sampling the initial condition randomly. Different initial conditions may result in different velocities, then different velocities are marked by different gray tones in the parameter space. The coexisting attractors are revealed by this algorithm. One can see from Fig. 3(a) that attractor $v = 0$ coexists with attractors $v = \pm \frac{1}{2}$ in the (γ, a) plane. Nontransporting attractor $v = 0$, which is globally attractive, exists in the whole parameter space. The nontransporting attractor $v = 0$ dominates the particular motion in the gray region. Attractor $v = -\frac{1}{2}$ dominates the transport in the black regime, while its counterpart $v = \frac{1}{2}$ governs the transport in the white regime. The black cross, which corresponds to the specific parameter values adopted in Figs. 1, 2, and 4, is located in the regime of the attractor $v = 0$, thus the particle is not transported at all but just oscillates around its equilibrium position. With the application of the second signal [see Fig. 3(b)], things change drastically. Beside the regimes dominated by the above attractors, new transport behaviors arise. Particularly, the dark gray regime in the left top of the figure exhibits negative velocity, while the black cross is also in this regime. Here the presence of the second signal has two roles. In one role it can induce directed transport in the direction opposite to the external bias in the nontransporting regime. In the other role, it reduces the

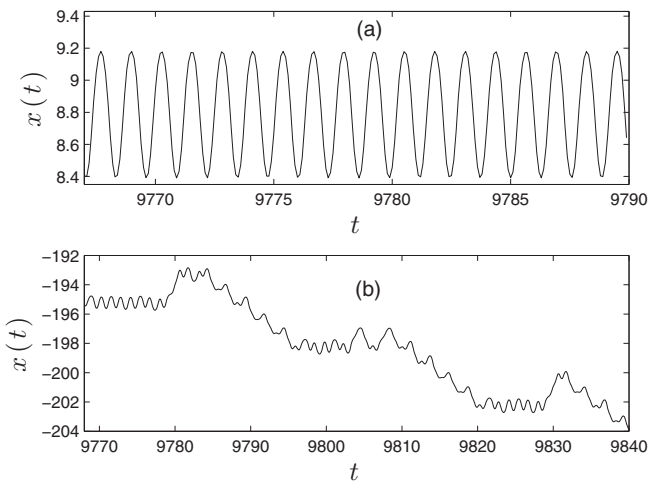


FIG. 4. The trajectory of the inertial particle for the (a) monochromatic and (b) biharmonic dynamics at $a = 4.2$, $\omega = 4.9$, $\gamma = 0.9$, $f = 0.12$, $\Omega = 1.6$, $\phi = 0$ and (a) $A = 0$, (b) $A = 0.05$.

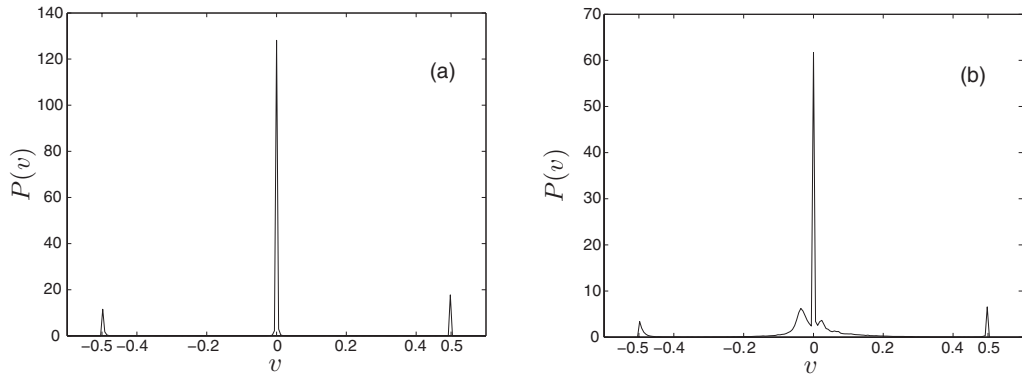


FIG. 5. The velocity probability distribution $P(v)$ of Fig. 3. The exact probability $P(v)$ in panel (a) for the three peaks (from left to right) read 11.56, 128.1, and 17.73. The exact probability $P(v)$ in panel (b) for the five peaks (from left to right) read 3.384, 6.242, 61.7, 6.626, and 6.557.

directed transport in a positive or negative direction induced by deterministic attractors.

The probability distribution $P(v)$ of the velocity v calculated in Fig. 3 is plotted in Fig. 5. For the case of the driving amplitude $A = 0$, the $P(v)$ possesses three peaks that locate in $v = 0, \pm\frac{1}{2}$, respectively. The three peaks are in accordance with the three coexisting attractors in Fig. 5. In the case of the driving amplitude $A = 0.05$, two additional peaks emerge around the origin, and the left peak is more obvious than the right peak. It is seen that the added signal is apt to favor transport in the negative direction in the nontransporting regime.

Although the ANM phenomenon in Fig. 2 is observed for fixed values of driving strength A and frequency Ω , it is not an exception and can emerge in a wide range of A and Ω . This point is confirmed in Fig. 6 by scanning the parameter space where it exhibits negative velocity. Within the regime of $A \in (0.02, 0.21)$ at $\Omega = 1.6$, the direction of the current is opposite to the applied bias f . The velocity $\langle v \rangle$ has a negative-valued minima at $A = 0.11$, which means the negative velocity can be maximized by choosing the proper driving amplitude. For $A > 0.21$, the particle displays normal transport. Under the regime of $\Omega \in (1.4, 2.2)$ at $A = 0.05$, the sign of $\langle v \rangle$ is opposite to f . This means the particle shows

the ANM feature, and the ANM is optimized at $\Omega = 1.5$. For $\Omega < 1.4$ or $\Omega > 2.2$, no transport occurs. Moreover, a kind of resonant activation (RA) arises in Fig. 6(b), where the average velocity possesses absolute peaks versus the oscillatory drive frequency [6,7].

To quantify the transport properties under the varying of amplitude A and frequency Ω , we plot the (A, Ω) plane in Fig. 7. The same method in Fig. 3 is adopted to generate Fig. 7. In Fig. 7, the anomalous transport opposite to small bias f exists in a wide range, just beyond the light gray region and the white region. When the frequency Ω exceeds some value, the gray level deepens, which means the presence of negative velocity against the small bias f . Meanwhile, the parameter values ($A = 0.05, \Omega = 1.6$) marked by a black cross are in the dark gray regime. This is consistent with the ANM phenomenon in Fig. 2. The maximally achievable velocities against the small bias can be improved by selecting the parameter values in the black regime.

The probability distribution $P(v)$ of the velocity v in Fig. 7 is plotted in Fig. 8. The probability distribution $P(v)$ has two peaks. The sharp peak which locates at $v = 0$ is induced by the attractor $v = 0$. The broad peak which locates around $v = -0.03$ reflects the ANM phenomenon induced by the additional signal.

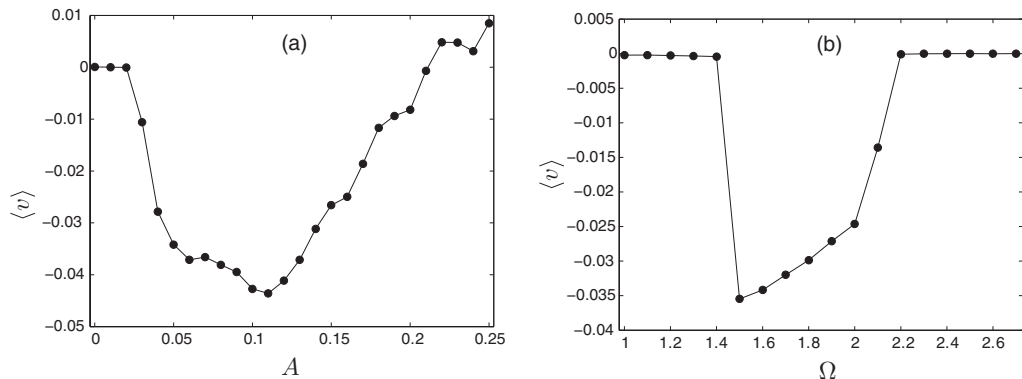


FIG. 6. The average velocity $\langle v \rangle$ as a function of A and Ω at $a = 4.2, \omega = 4.9, \gamma = 0.9, f = 0.12, \phi = 0$ and (a) $\Omega = 1.6$, (b) $A = 0.05$.

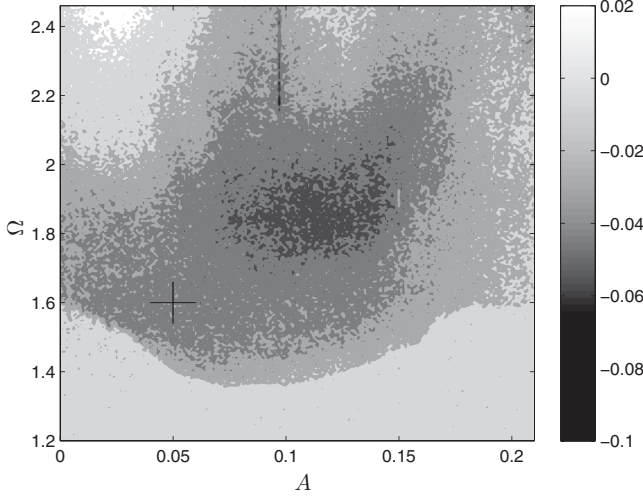


FIG. 7. The transport properties of a driven system in the parameter space (A, Ω) when the parameter values read $\gamma = 0.9$, $a = 4.2$, $\omega = 4.9$, $f = 0.12$, and $\phi = 0$. Different gray tones denote different velocities ($v > 0$). The white region exhibits normal transport while the light gray region does not exhibit transport behavior ($v = 0$), and other regimes display the anomalous transport feature ($v < 0$). Specific parameter values ($A = 0.05$ and $\Omega = 1.6$) in Figs. 1 through 4 are indicated by a black cross.

In the simulation results of Figs. 1 through 8, the phase shift ϕ is set at zero. The time-reversal invariance is persistent under this case. However, the nonzero ϕ induces the breaking of the time-reversal symmetry [31]. In Fig. 9, we have presented the ANM phenomenon for several values of phase shift ϕ . Varying ϕ just yields a slight influence on the ANM phenomenon. Since the driving amplitude A is very weak compared to a , the change of relative phase shift hardly affects the ANM phenomenon.

In our study, the system parameters are all of the order of magnitude of unity, which makes analytical studies extremely

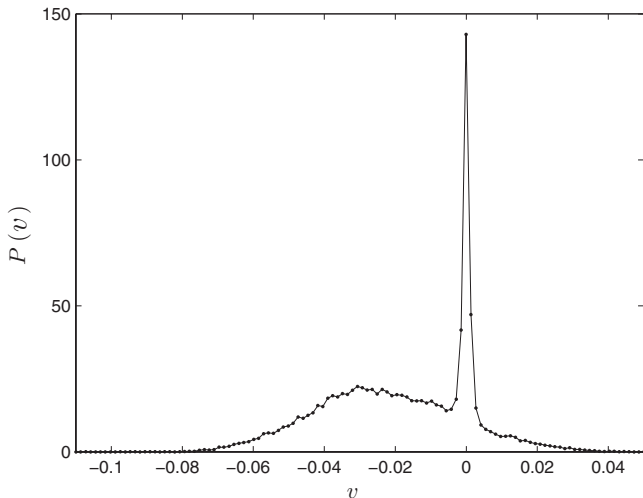


FIG. 8. The velocity probability distribution $P(v)$ of Fig. 7. The exact probability $P(v)$ for the two peaks (from left to right) reads 22.39 and 142.9.

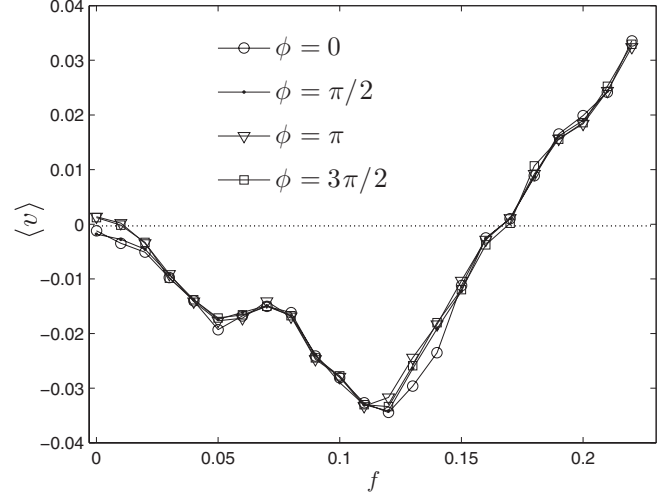


FIG. 9. The average velocity $\langle v \rangle$ versus f with different values of phase shift ϕ . The rest of the parameters are the same as those in Fig. 2. Dotted horizontal line corresponds to zero current.

difficult [16]. Known analytical tools, including a perturbational approach, become completely impossible. Numerical simulations become a reliable tool on modeling the ANM phenomenon [14–18].

III. CONCLUSION

The idea of a vibrational motor is put forward when the role of noise in a Brownian motor is replaced by a time-periodic force. An abnormal transport phenomenon termed absolute negative mobility (ANM) is investigated in a vibrational motor. For the regime where the ANM phenomenon is solely induced by a noise, the ANM can also be induced by a weakly periodic force. These theoretical results imply an alternative strategy for the control of the ANM phenomenon. Since the periodic driving is more controllable than the noise, the ANM observed here might shed light on many processes where different particle species or biology molecular should be sorted or separated. In addition, many other interesting transport phenomena, such as current reversal, desire further exploration in the vibrational motor. The present paper does not consider the influence of noise. This issue is the subject of our ongoing investigations.

ACKNOWLEDGMENTS

This work was supported by the National Natural Science Foundation of China (Grant No. 11165016), the program for Innovative Research Team (in Science and Technology) in the University of Yunnan Province and the Cultivation Foundation for Outstanding Doctoral Dissertation of Yunnan University.

- [1] P. Reimann, *Phys. Rep.* **361**, 57 (2002).
- [2] P. Reimann and P. Hänggi, *Appl. Phys. A* **75**, 169 (2002).
- [3] J. H. Li and S. G. Chen, *Phys. Rev. Lett.* **93**, 014102 (2004).
- [4] D. Wu and S. Zhu, *Phys. Rev. E* **73**, 051107 (2006).
- [5] P. Hänggi and F. Marchesoni, *Rev. Mod. Phys.* **81**, 387 (2009).
- [6] R. Gommers, P. Douglas, S. Bergamini, M. Goonasekera, P. H. Jones, and F. Renzoni, *Phys. Rev. Lett.* **94**, 143001 (2005).
- [7] J. H. Li and J. Łuczka, *Phys. Rev. E* **82**, 041104 (2010).
- [8] B. J. Keay, S. Zeuner Jr., S. J. Allen, K. D. Maranowski, A. C. Gossard, U. Bhattacharya, and M. J. W. Rodwell, *Phys. Rev. Lett.* **75**, 4102 (1995).
- [9] P. Reimann, R. Kawai, C. Van den Broeck, and P. Hänggi, *Europhys. Lett.* **45**, 545 (1999).
- [10] R. Eichhorn, P. Reimann, and P. Hänggi, *Phys. Rev. Lett.* **88**, 190601 (2002).
- [11] R. Eichhorn, P. Reimann, and P. Hänggi, *Phys. Rev. E* **66**, 066132 (2002).
- [12] R. Eichhorn, P. Reimann, and P. Hänggi, *Physica A* **325**, 101 (2003).
- [13] A. Ros, R. Eichhorn, J. Regtmeier, T. T. Duong, P. Reimann, and D. Anselmetti, *Nature (London)* **436**, 928 (2005).
- [14] L. Machura, M. Kostur, P. Talkner, J. Łuczka, and P. Hänggi, *Phys. Rev. Lett.* **98**, 040601 (2007).
- [15] D. Speer, R. Eichhorn, and P. Reimann, *Europhys. Lett.* **79**, 10005 (2007).
- [16] D. Speer, R. Eichhorn, and P. Reimann, *Phys. Rev. E* **76**, 051110 (2007).
- [17] M. Kostur, J. Łuczka, and P. Hänggi, *Phys. Rev. E* **80**, 051121 (2009).
- [18] M. Kostur, L. Machura, P. Talkner, P. Hänggi, and J. Łuczka, *Phys. Rev. B* **77**, 104509 (2008).
- [19] J. Nagel, D. Speer, T. Gaber, A. Sterck, R. Eichhorn, P. Reimann, K. Ilin, M. Siegel, D. Koelle, and R. Kleiner, *Phys. Rev. Lett.* **100**, 217001 (2008).
- [20] D. Speer, R. Eichhorn, and P. Reimann, *Phys. Rev. Lett.* **102**, 124101 (2009).
- [21] P. Hänggi, F. Marchesoni, S. Savelev, and G. Schmid, *Phys. Rev. E* **82**, 041121 (2010).
- [22] D. Hennig, *Phys. Rev. E* **79**, 041114 (2009).
- [23] M. Januszewski and J. Łuczka, *Phys. Rev. E* **83**, 051117 (2011).
- [24] J. Regtmeier, R. Eichhorn, T. T. Duong, P. Reimann, D. Anselmetti, and A. Ros, *Eur. Phys. J. E* **22**, 335 (2007).
- [25] P. S. Landa and P. V. E. McClintock, *J. Phys. A* **33**, L433 (2000).
- [26] V. N. Chizhevsky, E. Smeu, and G. Giacomelli, *Phys. Rev. Lett.* **91**, 220602 (2003).
- [27] C. G. Yao and M. Zhan, *Phys. Rev. E* **81**, 061129 (2010).
- [28] R. L. Kautz, *Rep. Prog. Phys.* **59**, 935 (1996).
- [29] P. Jung, J. G. Kissner, and P. Hänggi, *Phys. Rev. Lett.* **76**, 3436 (1996).
- [30] J. L. Mateos, *Phys. Rev. Lett.* **84**, 258 (2000).
- [31] D. Cubero, V. Lebedev, and F. Renzoni, *Phys. Rev. E* **82**, 041116 (2010).